FLEXURAL BEHAVIOR OF CONTINUOUS CONCRETE BEAMS PRESTRESSED

WITH BONDED AND UNBONDED TENDONS

By

EMILY E. POOLEY

A thesis submitted to the

School of Graduate Studies

Rutgers, The State University of New Jersey

In partial fulfillment of the requirements

For the degree of

Master of Science

Graduate Program in Civil and Environmental Engineering

Written under the direction of

Hani H. Nassif

And approved by

____

____

____

New Brunswick, New Jersey

January, 2020

ABSTRACT OF THE THESIS

FLEXURAL BEHAVIOR OF CONTINUOUS CONCRETE BEAMS PRESTRESSED WITH BONDED AND UNBONDED TENDONS

by EMILY E. POOLEY

Thesis Director:

Hani H. Nassif

The use of unbonded tendons in prestressed beams is becoming an increasing popular option for the repair and strengthening of bridges, high-rise buildings, and foundation systems. However, there has been an increase in load demands on these structures as well as the need for repair to damaged sections throughout the lifespan of the structure. Thus, the need for a new, more effective way to design these prestressed members to meet ever growing demand of these structures is evident.

The main objective of this study is to investigate the performance of continuous beams prestressed with both bonded and unbonded tendons, known as hybrid beams. This investigation included the casting and testing of three continuous high strength concrete (HSC) beams prestressed with hybrid tendons. The results of this study include number of cracks, load-deflection behavior and load-strain behavior as well as an analysis of available hybrid code equations in their ability to predict the behavior of such hybrid beams. Based on the analysis of the experimental results, it is shown that the current code equations do not accurately predict the stress at ultimate and there is a need to provide more simplified and accurate equations.

ACKNOWLEDGEMENTS

I’m extremely grateful to my advisor, Dr. Hani H. Nassif for his support and guidance and valuable insight throughout my thesis.

I would also like extend my sincere thanks to Dr. Hani Nassif, and Dr. Nicole Fahrenfeld, and Dr. Adi Abu-Obeidah for being on my committee and for their helpful comments.

Finally, I am extremely grateful to my parents and fiancée for their unwavering support throughout the entire project.

TABLE OF CONTENTS

LIST OF FIGURES

LIST OF TABLES

LIST OF SYMBOLS

A_{psB} Area of bonded prestressed reinforcement

A_{psU} Area of unbonded prestressed reinforcement

A_s Area of non-prestressed tensile reinforcement

A_s' Area of non-prestressed compressive reinforcement

b Width of the section

b_w Web thickness for flanged sections

c Neutral axis depth measured from extreme top concrete fiber

c_y Depth to neutral axis at yield of prestressed reinforcement

d_p Depth of the prestressed reinforcement measured from top concrete fiber

d_{psB} Depth of the bonded prestressed reinforcement measured from top concrete fiber

d_{psU} Depth of the unbonded prestressed reinforcement measured from top concrete fiber

E_c Modulus of elasticity of concrete

f Load Geometry Factor

f_c' Compressive strength of concrete

f_{cu} Strength of concrete taken from cube tests

f_{peU} Effective prestressing force in unbonded tendons

Δf_{ps} Change in ultimate stress

f_{ps} Ultimate stress

f_{psU} Ultimate stress of unbonded tendons

f_{pu} Tensile strength of prestressing tendons

f_{py} Yield stress of prestressing tendons

f_{se} Effective prestressing in tendons after losses

f_y Yield stress of non-prestressed reinforcement

h Height of the section

h_f Flange thickness of section

L Span length

l_i Length of tendon between anchorages (in)

$l_e^{'}$ Modified effective length

M Bending moment

N_s Number of plastic hinges at supports in an assumed failure mechanism crossed by the tendon between anchorages or discretely bonded points assumed as:

For simple spans………………………..0

End spans of continuous units………….1

Interior spans of continuous units……....2

w_{max} Maximum crack width

ω_p Prestressing reinforcement index

$\sum$ Total

β_1 Stress block reduction factor (ACI 318-08)

Δ Midspan deflection

ε_c Strain in the concrete

ϕ_{ps} Resistance factor the prestressing steel

ϕ_s Resistance factor for the non-prestressing steel

ϕ_c Resistance factor for the concrete

Ω_u Bond reduction coefficient

ψ Scaled plastic hinge length

CHAPTER I

1 INTRODUCTION

1.1 Overview

Prestressed concrete has been around since its invention in 1929 for various applications from structural members to thin shelled structures and stadium supports Dinges (2009). While concrete is usually weak in tension, the prestressing of the concrete allows it to overcome this weakness and carry higher loads with less deflection often with less cracks and longer sections.

Currently, there are two methods for prestressing, pre-tensioning and post-tensioning. The pre-tensioning process consists of tensioning the prestressing strands that are held between two anchors to a predetermined level. Then, once the concrete is cast on top of the strands and hardened, the tension from the hydraulic jack is released. By casting the concrete directly on the pre-tensioned strands, the stress that is released can be transferred to the concrete. This process mostly takes place in concrete plants and is then transported to the project location. With post-tensioning, on the other hand, the concrete is cast and hardened prior to the tendons being tensioned. To achieve this, ducts are placed inside the steel cage to provide a space for the tendon to pass through the beam after it is cast. The tendons can then be grouted inside the duct if there are to be bonded tendons or left alone if they are unbonded tendons. The grout provides corrosion resistance for which steel tendons are susceptible to.

Oftentimes, solely bonded or solely unbonded tendons are used in a prestressed beam. However, a combination, a hybrid, of bonded and unbonded beams is possible and is starting to be used as the research to their viability and behavior expands. Hybrid prestressed beams have been applied successfully on a handful of occasions in South Korea with development in the US underway (Nassif et al. (2004), Hwang et al. (1999) Han et al. (2003)). With the use of hybrid beams, even longer span lengths are possible with the same or shallower section depths.

1.2 Problem Statement

In beams prestressed with bonded tendons, the stress in the tendon can easily be found using force equilibrium and strain compatibility equations. In unbonded tendons, strain compatibility cannot be applied because the tendon does not form a bond and act as one as in a bonded tendon. Because of this, equations have been developed and implemented in codes internationally to describe the stress in the unbonded tendon. While there is, more or less, an accepted method for bonded and unbonded tendons independently, there is a striking lack of accurate and non-conservative equations to describe the ultimate moment capacity of a prestressed beam with hybrid tendons.

1.3 Research Significance

To calculate the ultimate moment resistance of beams prestressed with hybrid tendons, the stress in both the tendons at ultimate is required. Researchers have proposed equations to describe the tendon stress, but it has often resulted in complex and impractical equations. While some attempts have been made by AASHTO to conservatively estimate ultimate moment resistance of hybrid beams, none of these equations take into account the loading type or tendon profile. Both of these variables can have a dramatic effect on the ultimate moment capacity as a whole hybrid system and each tendon type (bonded or unbonded). Therefore, there is a need for a simple model that takes into account these variables to predict the stress in each tendon at ultimate.

1.4 Objective and Scope of Work

The primary objective of this research is to study the experimental flexural behavior of high-strength concrete beams prestressed with hybrid tendons, including the cracking behavior, the effect of loading type, and ultimate load carrying capacity of the unbonded and bonded tendons.

The research will focus on the following objectives:

1. This research will focus on the investigation of the use of hybrid tendons in continuous beams.

2. The experimental program will focus on understanding the behavior of hybrid tendons in continuous beams in terms of tendon profile and loading pattern.

1.5 Organization of the Thesis

The research work is described in six chapters:

Chapter 1 is the introduction which includes an overview of the research, problem statement, and objectives of the research.

Chapter 2 is a literature review that covers previous studies done on the use of unbonded tendons in prestressed beams as well as the use of hybrid tendons in prestressed beams. It will also cover code provisions for both unbonded and hybrid prestressed beams.

Chapter 3 is an analysis of current methods and their areas for improvement in use of unbonded and hybrid prestressed beams.

Chapter 4 is the experimental and testing program, including all the material properties, beam design, testing parameters, and instrumentation of beams.

Chapter 5 is the results section where the results of the experimental program are discussed. It will cover cracking behavior, load-deformation behavior, load-strain behavior, stress-strain behavior, and the application of code equations.

Chapter 6 is the conclusion of the study which summarizes the research, observations, and conclusions based on the results. It also offers some recommendations for the improvement of the current study.

CHAPTER II

2 LITERATURE REVIEW

2.1 Introduction

Concrete structures are particularly susceptible to environmental exposure that cause deterioration and change in time-dependent properties of the concrete (Kaewunruen (2019)). Kaewunruen (2019) concludes that environmental factors can influence material properties, structural performance, and service life. Beyond environmental factors, increases in acceptable live load per code designations and the difference between code standards and what loads are actually being applied (overweight trucks, etc.) has left previously safe structures in a precarious situation where they are unable to support these newly approved or actual loads (Gerges and Gergess, 2012). This deterioration causes an expensive problem that has engineers looking for a way to repair these structures as the alternate of complete replacement is cost prohibitive.

The Michigan Department of Transportation conducted a cost analysis study to find the economic impact of the repair of prestressed concrete I-beams versus total superstructure replacement. The Michigan DOT found that the cost of repair was only 35 to 69% of the total superstructure replacement cost (Needham (2000)). This study suggests that repair of prestressed members is in fact far more cost effective method of achieving acceptable structure conditions over total replacement. One method that has emerged as a way to increase the capacity of concrete bridges (reinforced concrete and pre-tensioned prestressed concrete) without replacing the original structure is to use external unbonded tendons to help meet load demands and address deterioration concerns of structural elements. The external unbonded tendons can help restore flexural capacity and respond to increases in load capacity while lessening factors such as deflection. Furthermore, external unbonded tendons can be used to repair girders that have damage to their internal steel prestressing strands when used as a means of replacement for these damaged tendons (Burningham et al. (2014)).

While there is tremendous use to external unbonded tendons, there is a significant drawback that makes this method one that must be researched further as to expand its capabilities or find an alternative. The main issue with steel unbonded tendons comes from the corrosion it experiences and its effect on useful lifespan (Burningham et al. (2014). Burningham et al. (2014) highlights potential methods to protect the steel prestressing strands from deicing salts and moisture, two of the biggest contributors to corrosion, but the focus of current research is on using fiber-reinforced polymer (FRP) materials because of its corrosion resistance properties. However, Nassif et al. (2003) have proposed an entirely different approach to the repair problem. Both papers concluded that existing prestressed concrete beams can be repaired through the use of hybrid beams. Nassif et al. (2003) argues that, “the use of fully unbonded and replaceable tendons in combination with bonded tendons would be more redundant and reliable system of post-tensioning. The additional spare ducts for unbonded tendons can be used to offset any loss of tendons over the lifetime of the structure.” This approach solves the issue of corrosion on unbonded steel tendons as well as addressing the need for increase in flexural capacity.

However, there is a significant knowledge gap when it comes to hybrid beams and their performance as prestressed beams as well as the implications on repairability of these members. In this study, an experimental program that investigates the overall performance of concrete beams prestressed with hybrid tendons will be proposed.

In this chapter, the experimental work completed by other researchers will be summarized and explained. The table below outlines the papers that will be discussed.

Table 2-1 Summary of references discussed in literature

Publications and reports	Unbonded	Naaman and Alkhairi (1991)
		Xu et al. (1995)
		Allouche et al. (1999)
		Harajli (1990)
		Hussien et al. (2012)
		Zhou and Zheng (2014)
		Maguire et al. (2016)
		Six (2015)
		Lou et al. (2016)
		Kim and Kang (2019)
		Zhou and Xie (2019)
	Hybrid	Nassif et al. (2003)
		Ghallab and Beeby (2001)
		Ghallab and Beeby (2005)
		Brenkus (2016)

2.2 Related Studies

The current study is building off of the experimental and analytical work conducted by Tanchan (2001), Nassif et al. (2003), Ozkul (2007), Unal (2011) and Abu-Obeidah (2017).

Tanchan (2001) conducted an experimental program of 9 rectangular simply-supported unbonded prestressed high strength concrete beams in flexure. All the beams were tested with a two-point loading system. The parameters investigated include area of prestressing strand, effective stress, span-depth ratio, and area of non-prestressing steel. Tanchan (2001) went on to develop a finite element model to predict the behavior of the unbonded tendons. Using available prediction equations and design codes and the finite element model, a comparison was completed and a new prediction equation for f_{ps} at ultimate was developed by using finite element modeling and experimental results. The proposed equation can be considered accurate when considering $c, L, and\ d_p$ only. The finite element model can be used to predict the overall behavior of the unbonded prestressed members.

Nassif et al. (2003) developed a finite element model using ABAQUS for the analysis of hybrid prestressed beams. Nassif et al. (2003) describes the model as being, "based on the structural idealization of the beam and the tendon along its longitudinal axis with an eccentricity." This can be described succinctly as an idealized trussed-beam model. Once the finite element model was developed, the experimental results of three unbonded specimens from a study conducted by Tanchan (2001) and Ozkul (2007) and two bonded specimens from Harajli (1985) were implemented in the model and a comparison for accuracy was made. The parameters that were considered in the comparison included deflection at cracking and ultimate, cracking load, ultimate load, stress increase and ultimate stress in the tendon. The authors found that the experimental results correlate extremely well to the model results. However, when the experimental results were compared to the ACI code equations, it was found that code equations were very conservative with the highest error average of 57%. Nassif et al. (2003) acknowledges a need for the development of equations to describe hybrid beams. Yet, the ACI code was able to conservatively estimate the ultimate capacity of hybrid beams with an average error of 17%. Nassif et al. (2003) concluded that the model developed can be used to predict the behavior of both externally and internally prestressed hybrid beams accurately and consistently.

Ozkul et al. (2008) aims to validate the model developed by Nassif et al. (2003) for unbonded prestressed beams as well as develop their own stress prediction equation. For the experimental program, Ozkul et al. (2008) cast 25 high-strength concrete (HSC), simply supported unbonded beams and compared the results, as well as experimental results from literature, with the results of the Nassif et al. (2003) model to validate the model. The parameters considered in the experimental program include deflection and strain in the prestressing strands, reinforcing steel and concrete. The parameters that were considered in the model included area of reinforcing steel, concrete strength, area of prestressing steel, effective prestress, and span-depth ratio. Ozkul et al. (2003) also completed an analytical study that allowed them to derive their prediction equation. The authors compared their prediction equation and the model to the experimental results and found both predicted stresses accurately with the model having the highest correlation of calculated-to-experimental ratio of 0.95 with a standard deviation of 0.04.

Unal (2011) developed a prediction equation for the stress at ultimate in unbonded tendons based off an analytical study of current research. The proposed equation it uses is the approach (Generalized Incremental Analysis (GIA)) utilized by Nassif et al. (2003) and

Ozkul et al. (2008) in their research. Once the equation was developed, the author used a large number of experimental results from literature to validate their equation as well as compare results of equations from literature and code equations. Unal (2011) found that their equation provides good accuracy with correlations factors of R = 0.93 and R = 0.75 for f_{psU} and Δf_{psU}, respectively. Unal (2011) found their equation can also be applied to unbonded or hybrid beams as well as internal or external tendons.

Abu-Obeidah (2017) conducted an experimental program including the testing of 15 high strength concrete beams that were prestressed with hybrid tendons. The parameters Abu-Obeidah considers include the depth of the tendons, area of the bonded tendons, area and material of the unbonded tendons, effective prestress, and span-depth ratio. A comprehensive analytical model using finite element analysis was developed to verify and validate the results from the experimental program in regards to load-deformation of the beams prestressed with unbonded tendons as well as stress increase in the unbonded tendon. Additionally, code equations and the proposed prediction equation by Unal (2011) are summarized and compared using the experimental data to a high degree of accuracy.

The following sections summarize the research recently conducted on unbonded and hybrid tendons in prestressed beams. Additionally, code equations for ultimate stress in the tendons will be discussed.

2.2.1 Studies on Beams Prestressed with Unbonded Tendons

Naaman and Alkhairi (1991) completed a state-of-the-art review of methods that were currently available to predict f_{ps} at ultimate in unbonded tendons of prestressed and partially prestressed beams for the purpose of computing their nominal bending moment resistance. Naaman and Alkhairi (1991) reviewed current studies and code equations and compared predicted versus experimental values of f_{ps} and found most equations were quite conservative. The authors went on to propose their own equation in the second part of this study. This was achieved by identifying the most critical variables in the analysis and incorporating them in the equation as well as the introduction of a bond reduction coefficient Ω_u to account for the difference in bonded and unbonded tendons. Because of this, the equation created was able to much more accurately predict f_{ps} at ultimate in comparison to the results from the review. The equation was recommended to replace the then current equations (18-4) and (18-5) in the ACI code (1990 version). The equations are as follows:

$$f_{ps} = f_{pe} + \Delta f_{ps} = f_{pe} + \frac{\Omega_u E_{ps} \epsilon_{cu} \left(\frac{d_p}{c} - 1\right) L_1}{L_2}$$

$$f_{ps} \leq 0.94 f_{py}$$

Where,

$\Omega_u = \frac{1.5}{\frac{L}{d_{ps}}}$ for one point loading

$\Omega_u = \frac{3.0}{\frac{L}{d_{ps}}}$ for third point or uniform loading

$L_1 = length\ of\ loaded\ span\ or\ sum\ of\ lengths\ of\ loaded\ spans, affected\ by\ the\ same\ tendon$

$L_2 = length\ of\ tendon\ between\ end\ anchorages$

Allouche et al. (1999) conducted a two part study on the factors that affect tendon stress in continuous unbonded prestressed concrete members. The first part focused on the literature review and a comparison of test results with code predictions. Part 2 of the study focuses on the creation and testing of a nonlinear numerical model used to predict the response of an unbonded, partially prestressed, continuous concrete beam. Together with an iterative moment-curvature approach, a numerical model using finite element method is created to calculate the increase in concrete strain at tendon height along the beam. The model was verified through a comparison of experimental and produced results across many loading situations and patterns. Allouche et al. (1999) concluded that their model provides an accurate method for response prediction for simply supported and continuous members prestressed with unbonded tendons. The authors also concluded that the loading pattern plays a large role in Δf_{ps} because it is related to how many plastic hinges can form for each loading pattern. “The larger the number of hinges, the larger is the increase in tendon stress,” concluded the authors. Furthermore, the change in tendon stress was directed by the type of loading (one point or two points per span). Based on their two part study, Allouche et al. (1999) proposed the following equation for predicting tendon stress at ultimate in members prestressed with unbonded tendons:

$$f_{ps} = f_{se} + \frac{1160}{(l'_e)(d_p - c_y)\left[1+\left(\frac{c_y}{d_p}\right)^2\right]} \qquad \text{(psi)}$$

Where

$f_{se} = effective\ stress\ in\ prestressed\ reinforcement\ (after\ all\ losses)$

$l'_e = \ modified\ effective\ length$

$c_y = depth\ to\ neutral\ axis\ at\ yield\ of\ prestressed\ reinforcement$

$d_p = \ effective\ depth\ of\ prestressed\ reinforcement$

Harajli (1990) investigated the influence of span-depth ratio on the predicted f_{ps} of unbonded prestressed concrete members using an analytical program they developed. The analytical program consisted of analyzing the strain distribution relationship for unbonded tendons and developing a strain compatibility relationship that predicts f_{ps} while considering the plastic hinge length and span-depth ratio. Harajli (1990) investigated the validity of the equation by comparing with experimental results and was able to correspond them accurately to beams with variable span-depth ratios, different tendon profiles, and different load applications. From analysis of experimental and analytical results, Harajli (1990) presents an equation to compute f_{ps} of unbonded prestressed concrete members at their normal flexural strength. However, this equation proved to be excessively conservative for members other than simply supported beams with single point loading.

$$f_{ps} = f_{pe} + \left(10{,}000 + \frac{f_c'}{100\rho_p}\right)\left(0.4 + \frac{8}{\frac{S}{d_p}}\right)$$

Where,

$f_{ps} \leq f_{py}$

$f_{ps} \leq f_{pe} + 60{,}000\ psi$

Hussien, et al. (2012) investigated both normal and high strength concrete with bonded and unbonded tendons. The experimental program consisted of nine beams; four of them were reinforced with bonded tendons, three were reinforced with unbonded tendons, and the last two were reinforced with non-prestressed reinforcement. Each beam was cyclically loaded to failure while recording the flexural capacity. The two main variables investigated in the study were concrete compressive strength and the tendon's prestressing index. From their experimental data, the authors concluded that in terms of ultimate deflection, initial stiffness and ductility, the partially prestressed beams with bonded tendons outperformed their unbonded counterparts. They went on to predict the ultimate stress in the unbonded tendons with accuracy up to 95% using the ACI 423.7-07, Naaman (2002) and Lee (1999) equations. However, because the ACI equation doesn't take into consideration of span-depth ratio, loading conditions, partial prestressing and non-prestressed reinforcement, there is room for improvement in the prediction of the ultimate stress results and ductility because of the important impact of these parameters.

Zhou and Zheng (2014) proposed a method to predict the ultimate stress in unbonded tendons in post-tensioned continuous beams. This method was derived from the experimental program consisting of 16 two-span continuous beams under static loading until failure. Their prediction model was derived from the equilibrium of the ultimate flexural capacity. It was then compared to the ACI 318-08 code and Chinese specificationJGJ 92-2004. In comparison to both other standards, their proposed prediction model was more accurate. This superiority was attributed to variables that were not included in the ACI 318-08 code and Chinese specification JGJ 92-2004, specifically those that affected the rotation capacity of plastic hinges. The equations take into account the span-depth ratio, the effect of the effective prestress force and the ratio of global reinforcement indexes of mid-span and inner support.

Simply supported:

$$\Delta\sigma_{pu} = \begin{cases} 663 - 1137\beta_p - 703\beta_s & \text{third point} \\ \left(560 - 1449\beta_p - 837\beta_s\right)\left(0.86 + \frac{2.4h}{L}\right) & \text{single point} \\ 631 - 1144\beta_p - 735\beta_s & \text{uniform} \end{cases}$$

Continuous:

$$\Delta\sigma_{pu} = \begin{cases} 677 - 1075\beta_p - 741\beta_s & \text{third point} \\ \left(632 - 1408\beta_p - 834\beta_s\right)\left(0.8 + \frac{2h}{L}\right) & \text{single point} \\ 659 - 1128\beta_p - 833\beta_s & \text{uniform} \end{cases}$$

Maguire et al. (2016) created a database of 253 unbonded prestressed beams to analyze Δf_{ps}. Using their database, the authors found the influence of certain material and geometric properties had on Δf_{ps} using a covariance analysis. Maguire et al. (2016) observed that there were several factors that correlated to simple span beams but not continuous beams. This indicates that prediction equations used for both simply supported and continuous beams may not be the most accurate method because of the correlation of certain variables to a simply supported beam may have a very weak correlation in a continuous beam. Furthermore, the prediction equations had relatively poor accuracy ($0.06 < R^2 < 0.16$) leading the authors to suggest modifications for scaled plastic hinge length ψ divided into different subsets (simple span, continuous, internally unbonded, and externally unbonded). The authors chose optimized ψvalues based on each subset and used a modified version of the AASHTO equation ($\Delta f_{ps} = \psi E_s \varepsilon_c \left(\frac{d_p - c_u}{L_e}\right)$) and were able to increase the accuracy to $R^2 = 0.27$ without increasing the complexity of the equation. Maguire et al. (2016) further proves the need to develop independent equations for continuous beams as well as address the differences in externally and internally unbonded tendons.

Six (2015) investigated the strand stress increase in four unbonded post-tensioned floor slabs. Six attempted to quantify the strand stress increase by using foil strain gauges at various locations on the tendon. However, the absolute stress strain profile was not able to be accurately determined because each exterior wire in the gauge experiences separate stress-strain relationships and cannot give a definite conclusion. However, the increase in strand stress was able to be accurately calculated due to similar changes seen across all wires. Six concluded that the ACI design method was conservative but inaccurate for all tests performed. Likewise, the AASHTO design method was also conservative but inaccurate for all tests performed. Six (2019) found that there was little correlation to factors that could influence the strand stress increase.

Lou et al. (2016) saw a gap in the knowledge of the characteristics of unbonded FRP tendons in continuous beams. Previously, the focus had been on simply supported beams only. Lou et al. (2016) developed a numerical model based on the finite element method to study these continuous beams. To verify the validity of their model, two specimens were created and tested. Lou et al. (2016) constructed two post-tensioned continuous beams subjected to third point loading. After testing, Lou et al. (2016) compared their results to those of the model and found the numerical model to match rather well. To further validate it, the experimental results from two simply supported beams from Harajli and Kanj (1991) were compared to the numerical model and again matched nicely. Lou et al. concluded that for calculating the ultimate stress in unbonded tendons in continuous beams, the ACI 318-11 equation is safe for ω_p (prestressing reinforcement index) greater than 0.048 but has a significant overestimation at low values of ω_p of 0.024. Furthermore, Lou et al. found that the ACI 318-11 code is conservative with respect to the prediction of permissible moment redistribution in continuous unbonded prestressed beams.

Kim and Kang (2019) focused their research on the applicability of using higher-strength strands (350 ksi) as compared to the standard (270 ksi) strands in unbonded post-tensioned beam members. Kim and Kang (2019) created and tested seven continuous post-tensioned beams which were loaded with 2 point loading on each span. The design was based on an existing building in Korea but built on a half scale for space saving purposes. The three parameters considered were strand type, profile height, and prestressing force. The authors concluded that all specimens, of all strand strengths (270 and 350 ksi) showed, regardless of other parameters such as prestressing force or profile height, to have corresponding ductile behavior. The ACI 318-14 equation was found to underestimate the member's actual strength. The authors used the experimental f_{ps} value to predict the actual member strength and found the equations from Naaman et al. (2002) and Harajli (2006) to be the most accurate while the AASHTO equation was most conservative.

Zhou and Xie (2019) investigate the flexural behavior of continuous CFRP-strengthened unbonded post-tensioned beams. These beams are widely used in practice as an option during retrofitting of existing structures. However, little research has been conducted. The authors looked to fill this gap in knowledge. Zhou and Xie (2019) created six two-span continuous beams, 5 of which were unbonded post-tensioned beams strengthened with CFRP laminate and 1 of which was a reinforced concrete beam strengthened with CFRP laminate. The authors studied the parameters of global reinforcement index at the inner support and midspan and the length of the single spans, ranging from 3-4.5m. The authors concluded that the global reinforcement indices of the two critical sections (at the inner support and the midspan) were vital for the flexural capacity. The authors found that the flexural capacity was positively correlated with moment redistribution. “The increase in the flexural capacity owing to the strengthening decreased substantially with increasing global reinforcement index” concluded Zhou and Xie (2019).

2.2.2 Studies on Beams Prestressed with Hybrid Tendons

As aforementioned, Nassif et al. (2003) developed a finite element model using ABAQUS to analyze concrete beams prestressed with hybrid tendons. This model paved the way for further studies on beams with hybrid tendons.

Ghallab and Beeby (2001) conducted an experimental program consisting of three hybrid simply supported beams under third point loading. The beams had an internal bonded steel strand that was pre-tensioned and an external unbonded FRP-Parafil Rope post-tensioned strand. Ghallab and Beeby (2001) focused on the behavior of the pre-tensioned beams once they were post-tensioned with the FRP. The authors compared the load deflection responses, cracking patterns, ultimate flexural strength and failure modes. Ghallab and Beeby (2001) concluded that FRP ropes externally can be used effectively to strengthen the prestressed concrete elements. They concluded this because they found that the cracking, beam stiffness and ultimate flexural strength showed improvement without sacrificing the ductility.

Improving on their previous work, Ghallab and Beeby (2005) went on to investigate the influence of several parameters on the increase in the ultimate strength in the external FRP ropes and external steel tendons. Additionally, they analyzed several codes for accuracy of their equations for ultimate stress in external tendons including the Eurocode (EC2), ACI 318-02, and British code (BS8110). Their experimental program consisted of nine beams with internal pre-tensioned bonded steel strands and external post-tensioned FRP Parafil Ropes. They tested all beams to failure with either one point or third point loading. Seven beams from Ghallab (2001) were also used in the analysis as well as others from literature. Ghallab and Beeby (2005) concluded that the parameters influenced the unbonded steel tendon's ultimate stress in the same way it affected the FRP ropes. Upon analysis of the code equations, they found that the Eurocode (EC2) is conservative, the British code (BS8110) is acceptable for FRP ropes but not steel tendons, and the ACI 318-02 code showed low accuracy when predicting external stress. Ghallab and Beeby (2005) recommended further research into other parameters that may influence to ultimate stress. They also recommended to change the ACI 318-02 equation to be considerate of high-strength concrete.

Brenkus (2016) created and tested three 40-ft simple span precast concrete I girders with unbonded tendons filled with flexible filler material and compared the results to a control specimen with a bonded tendon. Brenkus (2016) used a parabolic tendon profile. The filler material that was used was Civetea Cirinject-CP. Brenkus (2016) concluded that the ultimate strength is governed by the rotational capacity of the hinge region, regardless of being fully unbonded or a mix of bonded and unbonded. Brenkus also concluded that the AASHTO-LRFD equation for the predication of the hinge length was an over-estimation and therefore unconservative.

2.3 Code Equations

2.3.1 Unbonded Tendons

The ACI-318-14 (ACI (2014)) code equation is based on research by Mattock et al. (1971) and then later updated by Mojtahedi and Gamble (1978). It can be written as follows:

	For ln/h ≤ 35	For ln/h ≥ 35
The least of	$f_{ps} = f_{se} + 10000 + \frac{f_c'}{100\rho_p}$	$f_{ps} = f_{se} + 10000 + \frac{f_c'}{300\rho_p}$
	$f_{ps} = f_{se} + 60000$	$f_{ps} = f_{se} + 30000$
	$f_{ps} = f_{py}$	$f_{ps} = f_{py}$

Based off the work of Naaman et al. (2002), the ACI440.4R (ACI-440, 2004) code equation uses compatibility of strains (with the assumption that the tendon is bonded) and then applies a reduction factor Ω to account for the tendons being unbonded. The equation is as follows:

$$f_{ps} = f_{pe} + \Omega_u E_p \, \varepsilon_{cu}\left(\frac{d_p}{c} - 1\right)$$

Where,

$\Omega_u = \frac{1.5}{\left(\frac{L}{d_p}\right)}$ For one point loading

$\Omega_u = \frac{3.0}{\left(\frac{L}{d_p}\right)}$ For two point and uniform loading

AASHTO (2017) recommends, for rectangular or flanged sections, the following design equation:

$$f_{ps} = f_{se} + 900\left(\frac{d_p - c}{l_e}\right) \leq f_{py} \qquad \text{Eq. 5.6.3.1.1-1}$$

Where,

$$l_e = \left(\frac{2l_i}{2+N_s}\right) \qquad \text{Eq. 5.6.3.1.1-2}$$

$$c = \frac{A_{ps}f_{pu} + A_s f_y - A'_s f'_y - 0.85 f'_c \beta_1 (b - b_w) h_f}{0.85 f'_c \beta_1 b_w} \qquad \text{(for T-section behavior)} \qquad \text{Eq. 5.6.3.1.1-3}$$

$$c = \frac{A_{ps}f_{pu} + A_s f_y - A'_s f'_y}{0.85 f'_c \beta_1 b + k A_{ps}\left(\frac{f_{pu}}{d_p}\right)} \qquad \text{(for rectangular behavior)} \qquad \text{Eq. 5.6.3.1.1-4}$$

AASHTO (2017) recommends the following adjustments to the equations (Eq. 5.6.3.1.1-1) for ultimate moment capacity for unbonded tendons:

“In lieu of the detailed analysis described in Article 5.7.3.1.3a, the stress in the unbonded tendons may be conservatively taken as the effective stress in the prestressing steel after losses, f_{pe}. In this case, the stress in the bonded prestressing steel shall be computed using Eqs. 5.6.3.1.1-1 through 5.6.3.1.1-4, with the term $A_{ps}f_{pu}$ in Eqs. 5.6.3.1.1-3 and 5.6.3.1.1-4 replaced with the term $A_{psb}f_{pu} + A_{psu}f_{pe}$.

Where:

$A_{psb} = area\ of\ bonded\ prestressing\ steel\ (mm^2)$

$A_{psu} = area\ of\ unbonded\ prestressing\ steel\ (mm^2)$ "

$$f_{ps} = f_{se} + 900\left(\frac{d_p - c}{l_e}\right) \leq f_{py} \qquad \text{Eq. 5.6.3.1.1-1}$$

Where,

$$l_e = \left(\frac{2l_i}{2+N_s}\right) \qquad \text{Eq. 5.6.3.1.1-2}$$

$$c = \frac{A_{psb}f_{pu} + A_{psu}f_{pe} + A_s f_y - A'_s f'_y - 0.85 f'_c \beta_1 (b - b_w) h_f}{0.85 f'_c \beta_1 b_w} \quad \text{(for T-section behavior)} \qquad \text{Eq. 5.6.3.1.1-3}$$

$$c = \frac{A_{psb}f_{pu} + A_{psu}f_{pe} + A_s f_y - A'_s f'_y}{0.85 f'_c \beta_1 b + k\left(\frac{(A_{psb}f_{pu} + A_{psu}f_{pe})}{d_p}\right)} \quad \text{(for rectangular behavior)} \qquad \text{Eq. 5.6.3.1.1-4}$$

It is clear that there is a lack of equations to describe the unbonded tendon of a hybrid beam's behavior for ultimate moment capacity. Even when a code attempts to describe the behavior, it does so extremely conservatively. Because of this, there is a clear need for further investigation and experimentation on this topic.

CHAPTER III

3 EXPERIMENTAL PROGRAM

3.1 Introduction

The objective of the experimental program is to determine the effect of using both bonded and unbonded steel tendons in prestressed beams. Combining both bonded and unbonded tendons will give a longer span length with a smaller section.

A total of 3 beams were cast and tested in the Rutgers Civil Engineering Laboratory. The parameters that were considered in the program are:

1. Tendon profile
2. Loading type

The research focuses on two main parameters: the loading type (1 or 2 point loading) and tendon profile (1 or 2 point). Each beam was continuous and is equipped with strain gauges on the reinforcing steel for measuring the strain, a load is used to measure the force in the strand, and Linear Variable Differential Transducers (LVDTs) are used to measure deflection along the span as well as strain on the top and side of the concrete beams. All data is collected using a CR3000 datalogger. High-strength concrete design with target strength of 12 ksi is used. To illustrate the experimental program, a flow chart is included below. Each task will then be further explained in detail. As shown in the flow chart, the experimental work will go through three phases. These phases are mechanical testing, building and casting, and testing.

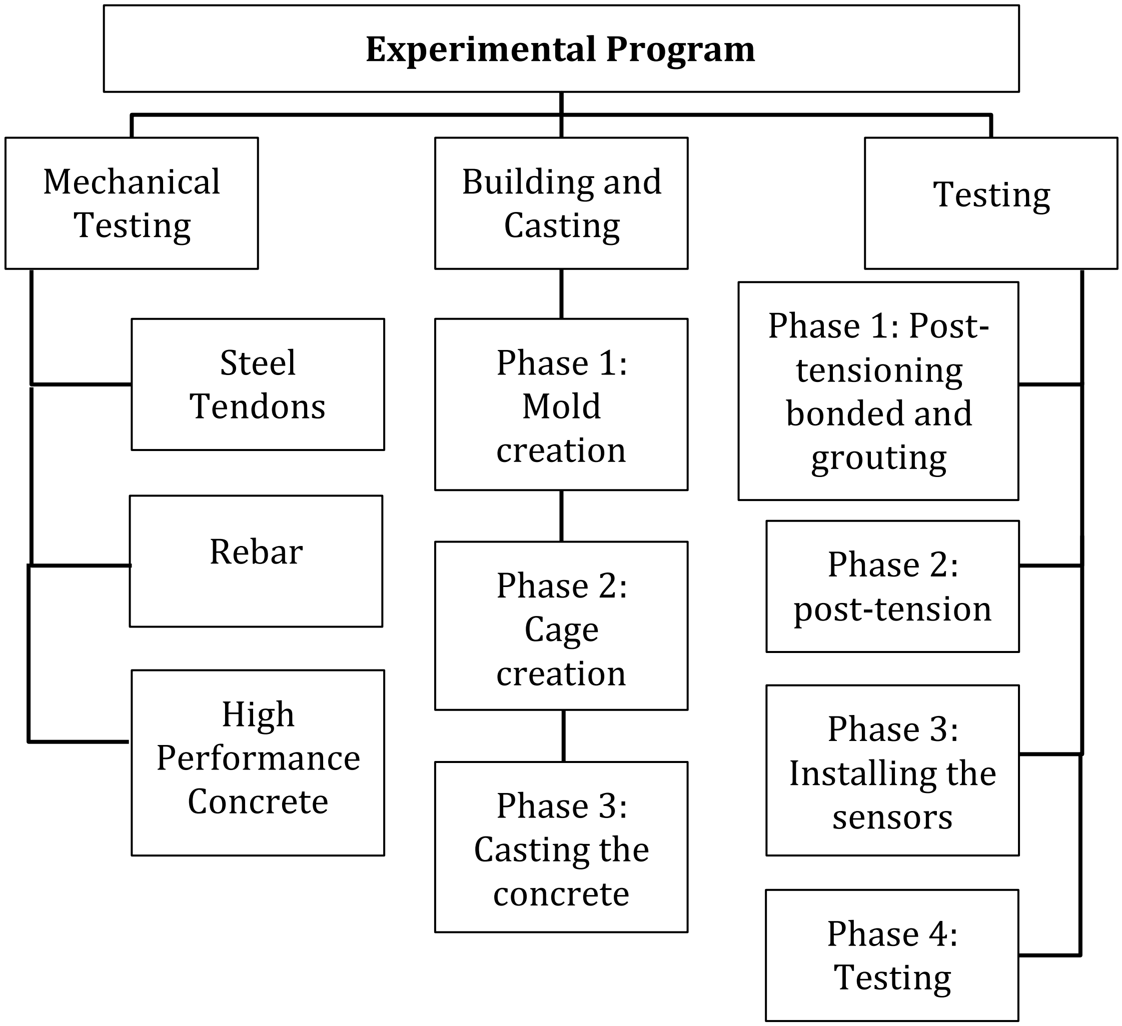

Figure 3-1 Experimental program flow chart

3.1.1 Mechanical Properties Test

3.1.1.1 High Performance Concrete

The concrete mix design proposed was mixed and tested in the lab. The proportions of the mix are given in table 3.1**.** The mix contains silica fume which was used to create the high performance concrete mix that meet all the minimum standards of such a mix. The 28 day strength results are summarized in table 3.2. The mix achieved around 13,217 psi on day 28. This corresponds to 4655 psi modulus of elasticity. The final selection of the mix design was primarily chosen for its 28 days compressive strength but also factored workability in.

Table 3-1 Concrete mix design

Mix Design		
Material	**Weight**	**Volume**
Cement	513 lb	2.61 ft^3
Silica Fume	51.29 lb	0.371 ft^3
Rock (3/8”)	781.88 lb	4.43 ft^3
Sand	431.58 lb	2.64 ft^3
Water	151.72 lb	2.43 ft^3
HRWR	2920 mL	0.1 ft^3
Total		12.58 ft^3

Table 3-2 Concrete mechanical properties

Age	Compressive (psi)	Tensile (psi)	Modulus of elasticity (psi)	Cracking strain (με)
1 days	9375	667	4308	155
3 days	9753	707	4213	168
7 days	10669	673	4528	148
14 days	12022	700	4823	145
28 days	13217	776	4655	166
56 days	14252	498	4747	105

3.1.1.2 Prestressing Steel

Grade 270 seven-wire stress relieved strands were used in this experimental program. The diameter of all strands was 0.5 inches which has a nominal area of 0.153 in^2. The yield strength, ultimate stress, and modulus of elasticity for the 0.5” diameter strands were 265, 300, 33, 125 ksi, respectively.

3.1.1.3 Rebar

Grade 60 rebar was used in this experimental program. Two sizes of rebar were used, #2 and #3. The nominal area of size #2 and #3 are 0.049 and 0.11 in^2 respectively. The minimum yield strength is 60,000 lbs/in^2. The modulus of elasticity is 29,000 ksi.

3.1.2 Building and Casting Process

3.1.2.1 Phase 1: Building the Mold

The first phase of constructing each beam was to create the mold for the concrete to be poured in. Two different molds were used for three beams, with the second mold being cleaned and reused. The first mold was a T beam with a 2’ flange on the bottom as to make it an I section only at the middle. The second and third beams were true T beams. Each mold was constructed of ¾” plywood. Prior to casting, a waterproofing mixture was applied to the mold to aid in the demolding process.

Figure 3-2 Mold construction

3.1.2.2 Phase 2: Building the Cage

The second phase of constructing each beam was to create the steel cage. The steel cages were constructed from #2 and #3 rebar that was held together with rebar ties. A typical cross section is shown below in figure 3.3. Additionally, foil strain gauges were attached to the cage for use during testing. Furthermore, the tendon profile was constructed.

Using ½” diameter CPVC pipe for the unbonded tendon and 1 ¼” tubing for the bonded tendon, the tendon profile was created according to the beam specifications. All of the beam properties are described intable 3.3 below. The naming structure of the beams describes what number beam (B#), what type of loading (L#), and what type tendon profile (T#).

Table 3-3 Beam Properties

Beam No.	Positive Moment Section							
	Non-Prestressing Reinforcement				Bonded using Grout		Unbonded	
	A_s (in^2) (bot)	d_s (in)	A_s' (in^2) (top)	d_s' (in)	A_{psB} (in^2)	d_{psB} (in)	A_{psU} (in^2)	d_{psU} (in)
B1-L2-T1	0.22	9.25	0.22	0.9	0.058	8.5	0.058	7
B2-L1-T1	0.22	9.25	0.538	0.9	0.058	8.5	0.058	7
B3-L2-T2	0.22	9.25	0.538	0.9	0.058	8.5	0.058	7
Beam No.	Negative Moment Section							
	Non-Prestressing Reinforcement				Bonded using Grout		Unbonded	
	A_s (in^2) (bot)	d_s (in)	A_s' (in^2) (top)	d_s' (in)	A_{psB} (in^2)	d_{psB} (in)	A_{psU} (in^2)	d_{psU} (in)
B1-L2-T1	0.538	9	0.22	0.75	0.058	7.125	0.058	8.875
B2-L1-T1	0.538	9	0.22	0.75	0.058	7.125	0.058	8.875
B3-L2-T2	0.538	9	0.22	0.75	0.058	7.125	0.058	8.875
Beam No.	Tendon Profile			Cross Section		Loading		
B1-L2-T1	harped-1-point			T-section with middle flange		2 point		
B2-L1-T1	harped-1-point			T-section		1 point		
B3-L2-T2	harped-2-point			T-section		2 point		

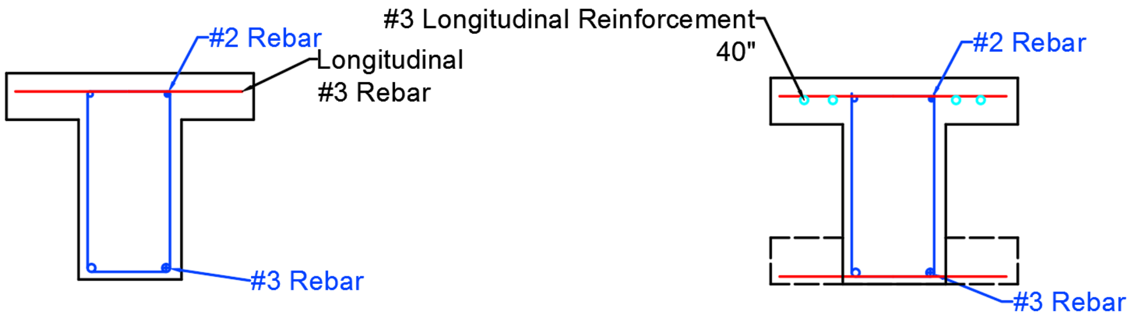

Figure 3-3 Reinforcement design

Figure 3-4 Tendon profile creation

3.1.2.3 Phase 3: Casting the Concrete

The third phase of constructing each beam was to cast the concrete. Each beam was mixed to ASTM standards. Each beam was mixed individually to ensure proper mixing. Additionally, enough cylinders and prisms were cast for each beam to carry out mechanical properties testing.

(a) (b)

Figure 3-5 Testing strain gauges after casting (a) and completely casted beam (b)

3.1.3 Testing

3.1.3.1 Phase 1: Post-tensioning bonded and grouting

Once the beam has aged for 28 days, the bonded tendon can be post-tensioned and grouted. After inserting grout caps to resist grout leakage, the bonded tendon can be jacked using the hydraulic jack to the required $\frac{f_{pu}}{f_{pe}}$ ratio (usually 0.7) or around 12 kips of jacking. Once the tendon is fully jacked and the load is stable, the grouting process can begin. After mixing the grout in a 5 gallon bucket, the grout is then raised in the bucket using the crane. The grout flows through the tube in the bottom of the bucket and is transferred to the bonded tube in the beam via a connection between the grout tube and the bonded tube.

Once the grout starts rising in the end zone tubes, the bucket can be lowered since the grout has spread throughout the beam.

3.1.3.2 Phase 2: Post-tensioning unbonded

At least seven days after grouting, since it takes this long to cure, the post-tensioning of the unbonded tendon can occur. Much like the bonded tendon, the unbonded tendon is jacked using the hydraulic jack to the required $\frac{f_{pu}}{f_{pe}}$ ratio (0.7) (Figure 3.6). Once the load is reached and stabilized, the unbonded tendon is jacked and the sensors can be installed.

Figure 3-6 Tendon anchoring set up

3.1.3.3 Phase 3: Install sensors

An important aspect of testing the beams is the installation of the sensors to take data during the testing process. Several different kinds of sensors were used to monitor various aspects of the beam during testing. Included in these are foil strain gauges, linear voltage displacement transducers (LVDTs), and load cells. The location of each sensor is indicated in the diagram below. Table 3.4 summarizes each sensors purpose.

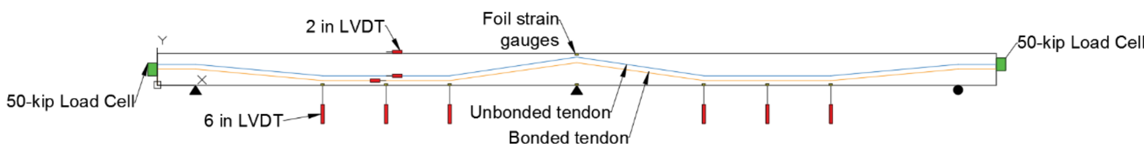

Figure 3-7 Strain measuring sensor locations

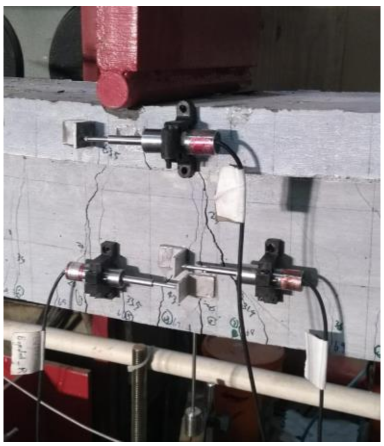

(a)

(b)

Figure 3-8 2" LVDTs (a) and foil strain gauges (b)

Table 3-4 Sensor details and purpose

Sensor details	**Reason**
Linear Variable Differential Transformer (LVDT) 	The LVDTs were supplied by RDP. Several lengths of LVDTs were used. These include #, 6”, and 2”. The LVDTs measure the deflection at critical locations as well as measure the strain at the beam’s extreme fiber.
250 kN Load Cell 	The 50-kip capacity load cells are used to monitor the load in tendons during jacking and testing.
Strain Gauge (Vishay) 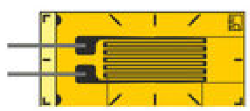	Foil strain gauges were attached to the flexure reinforcing bars at critical points along the span.

3.1.3.4 Phase 4: Testing

Once the tendons are post-tension and the sensors are installed, the testing process can begin. Beams were tested until failure under 1 point and 2 point loading per span depending on the design criteria. Data is collected from the sensors and cracks are monitored and photographed as they appear throughout the testing process.

(a)

(b)

Figure 3-9 2 Point loading setup (a) and Beam after failure (b)

CHAPTER IV

4 RESULTS

4.1 Introduction

The experimental results of three beams that were outlined in chapter III are explained in detail. The results discussed in this chapter are divided into three sections: overall behavior, load deformation behavior and application of code equations. The overall behavior includes reinforcing steel and concrete as well as crack width and number of cracks and unbonded and bonded f_{pe} and f_{ps}. The load deformation section includes the deflection at L/3, L/2, and 2L/3, the stress and strain in the strands. The application of code equations include the ACI 318-14 and AASHTO equations. Analysis and discussion for each result will be presented.

4.2 Overall Behavior

4.2.1 Cracking Behavior

Cracking occurs when principal tensile stresses exceed the tensile strength of the concrete. Then the tensile stress is transferred to the reinforcing steel from the concrete. As the load increases and the stress correspondingly increases, the crack will widen as the reinforcing steel elongates under stress. This pattern continues until failure of the beam or crushing of the concrete, whichever comes first.

During the testing of each beam, the number of cracks and crack widths were recorded as they appeared as well as re-measured at certain predefined points. To record the crack, a small camera capable of 200x magnification was connected to a laptop and a picture was recorded. For each crack recorded, the crack was assigned a number, a load when it occurs, and a crack width after the fact.

The first crack occurred at 25, 28.5, and 21.5 kips in beams B1-L2-T1, B2-L1-T1, and B3-L2-T2, respectively. This correlates to the ultimate load achieved where B3-L2-T2 had the lowest ultimate load if 43.78 kips and lowest initial cracking load and B2-L1-T1 had the highest ultimate load of 64.65 kips and highest initial cracking load. The number of cracks also correlated to ultimate load. Beams B1-L2-T1 and B2-L1-T1, with higher ultimate load of 64.56 and 64.65 kips respectively, had 52 and 57 cracks, respectively whereas beam B3-L2-T2, with lower ultimate load, only had 42 cracks. Because B3-L2-T2 had a significantly lower ultimate load which was inconsistent with other results, the beam would need to be re-designed repeated experimentally before any publications and will be designated with a * to signify this.

The maximum crack width was also investigated at 75% of the ultimate load as beyond this point, the data can become unreliable. The crack widths were 0.171, 0.103, and 0.34 mm in beams B1-L2-T1, B2-L1-T1, and B3-L2-T2* respectively. All of these cracks were recorded at the positive moment. Beams B1-L2-T1 and B2-L1-T1 had higher ultimate loads and initial crack loads so the crack widths didn’t develop as far as Beam B3-L2-T2* at 75% of the ultimate load. The results can be seen in table 4.1.

Table 4-1 Crack widths at 75% Ultimate

Beam Number	$w_{max}(in)$ at 75% Ultimate	Ultimate Load (kips)
B1-L2-T1	0.171	64.56
B2-L1-T1	0.103	64.65
B3-L2-T2*	0.34	43.78

4.2.2 Bonded and Unbonded f_{pe} and f_{ps}

Both bonded and unbonded tendons experience a different f_{pe} andf_{ps}. The bonded f_{pe} is somewhat close in value across all the beams. The bonded f_{pe} can be changed by the amount of prestressing that was induced prior to grouting. The f_{pe} for the unbonded tendon is relatively close across all beams. Also, the stress at ultimate was measured using load cells. The load cells were placed on the tendon as part of the anchorage setup before prestressing each tendon so the load in the tendons could be monitored. The load cells were left on the tendons during testing to monitor the change in load throughout the test until failure. There was little change in the bonded tendon because the tendon was held in place by the grout. The unbonded tendon experienced more change because it was free within the duct. The values of the effective stress and the stress at ultimate were calculated using the load in each tendon's load cell at the time of prestressing and at the ultimate load, respectively. The results for the effective stress and the stress at ultimate can be seen in Tables 4-2 and 4-3, respectively.

Table 4-2 Effective Stress in Bonded and Unbonded Tendons, fpe

Beam	Bonded/Unbonded	f_{pe}
B1-L2-T1	Bonded	210.56
	Unbonded	155.45
B2-L1-T1	Bonded	199.94
	Unbonded	162.01
B3-L2-T2*	Bonded	191.84
	Unbonded	151.60

Table 4-3 Stress in Bonded and Unbonded Tendons at Ultimate, fps

Beam	Bonded/Unbonded	f_{ps}
B1-L2-T1	Bonded	194.34
	Unbonded	263.22
B2-L1-T1	Bonded	202.54
	Unbonded	249.80
B3-L2-T2*	Bonded	239.95
	Unbonded	226.09

4.3 Load-Deformation Behavior

During testing, the load-deflection relationship and load-strain relationship were measured. The observations and results of these deformations will be discussed.

4.3.1 Load-Deflection Relationship

To correlate deflection with load, the deflection was measured at 2-3 locations on each span during testing until failure using LVDTs. The deflection taken at midspan (L/2) and deflection taken at one third span (L/3) are shown in figure 4.1 below.

It was observed that the tendon profile and loading combination of the prestressed strands affects the deflection of the beam at midspan. Beams B1-L2-T1 has the highest deflection followed by beam B3-L2-T2*. Both of these beams have the same loading and tendon profile (1-point loading and 1-point tendon profile or 2-point loading and 2-point tendon profile). The deflection at L/3 also has similar results where the highest deflection is found in B1-L2-T1.

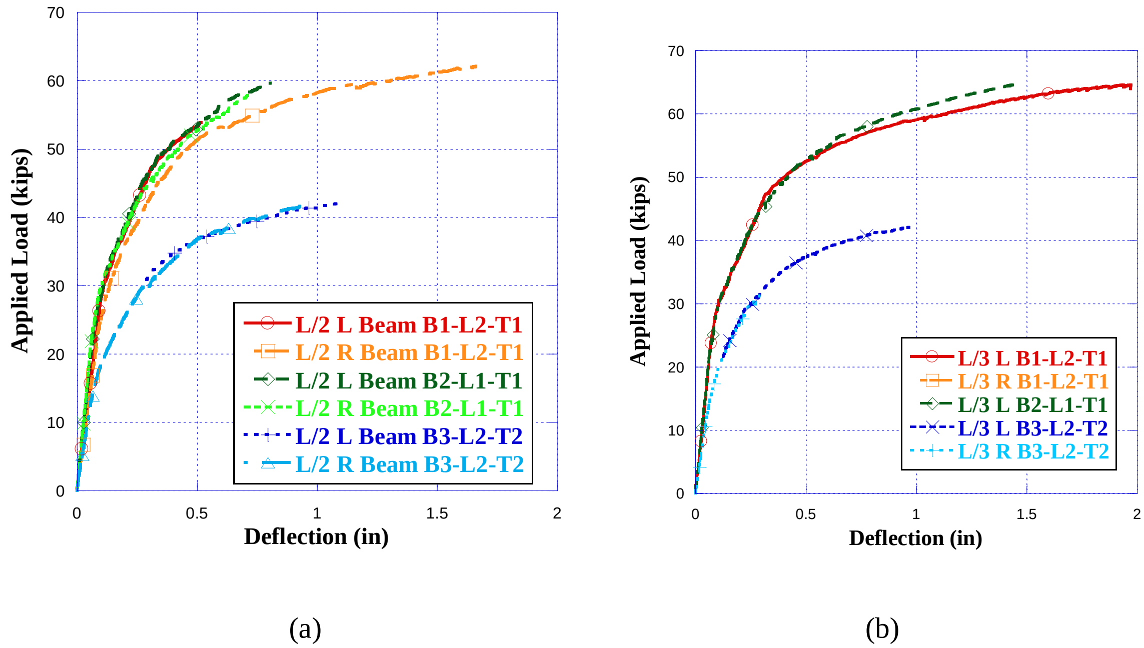

Figure 4-1 Deflection at L/2 (a) and Deflection at L/3 (b)

Furthermore, the deflection for each beam was plotted separately and can be seen below in figures 4.2 and 4.3. In all of the beam, the maximum deflection was at L/3.

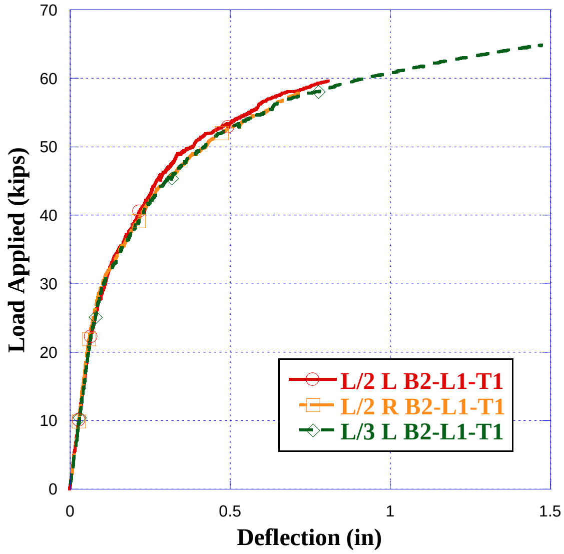

S

(a) (b)

Figure 4-2 B1-L2-T1 Deflection (a) and B2-L1-T1 Deflection (b)

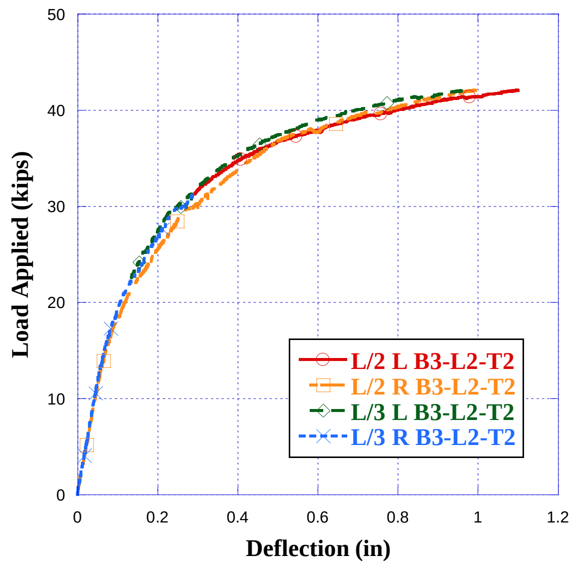

Figure 4-3 B3-L2-T2 Deflection

The location of the maximum deflection can be correlated to the tendon profile. Both beams B1-L2-T1 and B2-L1-T1 have a harped 1-point tendon profile and had the maximum deflection at L/3. Beam B3-L2-T2 has a harped 2-point tendon profile and had the maximum deflection at L/2. This correlation shows that the maximum deflection doesn't occur at a harping point in any of the beams. Table 4.3 shows the deflection progressively throughout testing.

Table 4-3 Deflection throughout testing

B1-L2-T1	Load (kip)	L/3 R	L/2 R	2L/3 R	L/3 L	L/2 L
Cracking	25	0.07	0.1	0.09	0.08	0.09
Yielding (non-prestressed reinforcement)	38.97	0.22	0.25	0.20	0.22	0.22
75% Ultimate	48.45	0.39	0.41	0.32	0.35	0.34
Yielding (bonded Tendon)	52.66	0.57	0.57	0.44	0.52	0.48
Ultimate	64.57	3.10	-	-	1.97	-

B2-L1-T1	Load (kip)	L/3 R	2L/3 R	L/2 R	L/3 L	L/2 L
Cracking	28.5	0.001	0.10	0.09	0.10	0.1
Yielding (non-prestressed reinforcement)	37.04	0.01	0.19	0.19	0.19	0.18
Yielding (bonded)	40.18	0.01	0.22	0.23	0.23	0.22
75% Ultimate	48.31	0.02	0.34	0.37	0.37	0.33
Ultimate	64.65	0.01	-	-	1.45	-

B3-L2-T2*	Load (kip)	L/3 R	L/2 R	2L/3 R	L/3 L	L/2 L
Cracking	21.5	0.13	0.11	0.11	0.13	0.05
Yielding (non-prestressed reinforcement)	26.80	0.20	0.17	0.17	0.19	0.14
75% Ultimate	32.83	0.33	0.28	0.28	0.32	0.34
Yielding (bonded)	41.72	-	0.71	0.71	0.93	1.06
Ultimate	43.78*	-	0.9	0.90	1.20	1.40

4.3.2 Load-Strain Relationship

During testing, the change in strain was measured in top concrete fibers as well as at tendon height on the side of the beam at the maximum moment location through LVDTs. Additionally, the strain was measured on the non-prestressed steel using strain gauges.

It is observed that the beams with the same tendon profile and loading type (Beams B1-L2-T1 and B3-L2-T2*) experience significantly more flexural reinforcement strain which can be seen in figure 4.4..

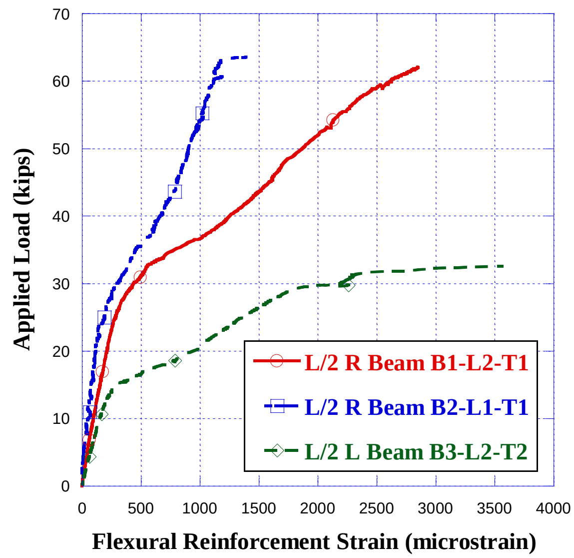

Figure 4-4 Load vs. Flexural Reinforcement Strain

4.3.3 Stress and Strain in Prestressing Steel

The stress in the prestressed tendons was also measured using a 50 kip load cell (Roctest) on the unbonded tendon during testing. It was observed that the strain in the prestressing steel follows the same pattern as when measured using the Geokon load cell. The beams with 2-point loading (Beams B1-L2-T1 and B3-L2-T2*) demonstrate higher flexural reinforcement strain. The deflection was greatest in beams B3-L2-T2* and B1-L2-T1 which can be attributed to having the same loading type (2-point).

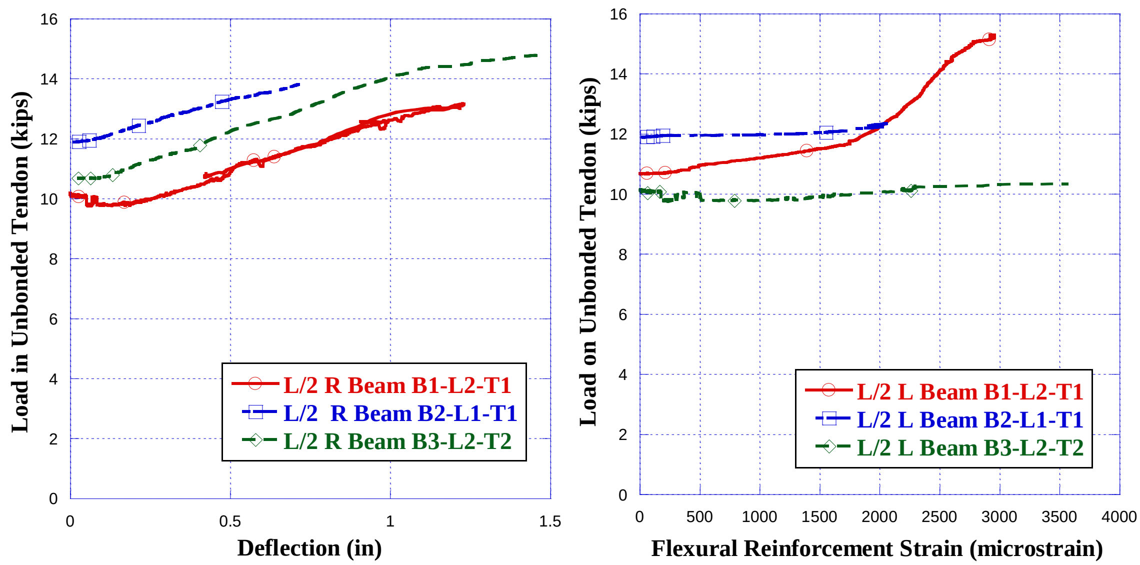

(a) (b)

Figure 4-5 Unbonded Load vs. Deflection (a) and Unbonded Load vs. Flexural Reinforcement Strain (b)

4.4 Application of Code Equations

4.4.1 ACI 318-14 Code Equation

ACI 318-14 offers a set of equations to calculate fps based on ln/h ratio. The equations are shown below.

	For ln/h ≤ 35	For ln/h ≥ 35
The least of	$f_{ps} = f_{se} + 10000 + \frac{f_c{}'}{100\rho_p}$	$f_{ps} = f_{se} + 10000 + \frac{f_c{}'}{300\rho_p}$
	$f_{ps} = f_{se} + 60000$	$f_{ps} = f_{se} + 30000$
	$f_{ps} = f_{py}$	$f_{ps} = f_{py}$

The results of using this equation are shown in Table 4-4. However, there are several problems with using this set of equations for hybrid tendons. There is no inclusion of bonded tendons in the equation anywhere, it is solely for unbonded tendons. In order to calculate ρ_p a combination of A_{psU} and A_{psB} had to be taken in lieu of any variables dedicated to each. Additionally, the average d_p had to be taken as there was not a separate variable for d_{pB} and d_{pU}. These issues make it a non-viable option for the design of hybrid tendons.

Table 4-4 Predictions for fps at Ultimate using ACI 318-14 Equation

Least of	
f_{ps} (kips)	**226.11**
	276.00
	243.00

4.4.2 AASHTO Equations

The only code that offers any commentary with supporting equations that include hybrid beams is AASHTO-LRFD Bridge Design Specifications (2018). To account for both bonded and unbonded tendons in hybrid beams, the $A_{ps}f_{pu}$ term in Eqs. 5.6.3.1.1-3 and 5.6.3.1.1-4 replaced with the term $A_{psb}f_{pu} + A_{psu}f_{pe}$.

$$f_{ps} = f_{se} + 900\left(\frac{d_p - c}{l_e}\right) \leq f_{py} \qquad \text{Eq. 5.6.3.1.1-1}$$

Where,

$$l_e = \left(\frac{2l_i}{2+N_s}\right) \qquad \text{Eq. 5.6.3.1.1-2}$$

$$c = \frac{A_{psb}f_{pu} + A_{psu}f_{pe} + A_s f_y - A'_s f'_y - 0.85 f'_c \beta_1 (b - b_w) h_f}{0.85 f'_c \beta_1 b_w} \quad \text{(for T-section behavior)} \quad \text{Eq. 5.6.3.1.1-3}$$

$$c = \frac{A_{psb}f_{pu} + A_{psu}f_{pe} + A_s f_y - A'_s f'_y}{0.85 f'_c \beta_1 b + k\left(\frac{A_{psb}f_{pu} + A_{psu}f_{pe}}{d_p}\right)} \quad \text{(for rectangular behavior)} \quad \text{Eq. 5.6.3.1.1-4}$$

When applying these equations to the experimental beams, the results satisfy the equation. However, there are several issues with substituting the new terms in. The first issue comes from the d_p term. There is no consideration of bonded and unbonded depths being different from each other or how much each tendon contributes. To calculate d_p, the average depth of both bonded and unbonded was taken and used but is not necessarily fully accurate as recommended. Another problem with the new equations is the calculation of f_{pe}. Both the bonded and unbonded tendons have separate f_{pe} values but the equation only requires one, total value. To account for this, the average prestressing force between the two tendons was used as recommend. However, there is no evidence to say that the prestressing force contributes equally in bonded and unbonded beams. The results of using the AASHTO equation are seen in Table 4-5.

Table 4-5 Predictions of fps at Ultimate using AASHTO equation

Beam Number	f_{ps} **(kips)**	f_{py} **(kips)**
B1-L2-T1	240.57	243
B2-L1-T1	240.54	
B3-L2-T2	240.45	

When comparing ACI 318-14 to AASHTO (2018) it is clear that the AASHTO equation provides better results because it takes into account that the bonded and unbonded tendons are different. However, for the reasons listed above, there is still a room for improvement. The experimental f_{ps} was calculated from the ultimate load in the unbonded tendon. A comparison of the difference between these equations with the experimental results can be seen in Table 4-6.

Table 4-6 Comparison of Code Equations with experimental results for f_{ps} in the unbonded tendon at ultimate

Beam Number	Experimental f_{ps} (kips)	AASHTO f_{ps} (kips)	Percent Difference of Experimental and AASHTO f_{ps} (%)	ACI 318-14 f_{ps} (kips)	Percent Difference of Experimental and ACI 318-14 f_{ps} (%)	f_{py} (kips)
B1-L2-T1	263.22	240.57	+9.42	226.11	+16.41	243
B2-L1-T1	249.80	240.54	+3.85	226.11	+10.47	
B3-L2-T2	226.09	240.45	-5.97	226.11	-0.01	

CHAPTER V

5 SUMMARY AND CONCLUSIONS

5.1 Summary

Hybrid beams are at the forefront of research in the prestressed industry. It is critical that the behavior of these beams be investigated to increase its potential for use in cutting edge designs moving forward. However, there is little research on hybrid beams and even less on continuous hybrid beams. This study presents an overall review of the available literature and an experimental program investigating several parameters. The literature review summarized the behavior of both unbonded and hybrid beams including experimental and analytical work and the most up to date code equations. An experimental program was developed to observe the effect of tendon profile and loading type on continuous hybrid beams. The results of the experimental program are presented in Chapter IV. The experimental results include number of cracks, crack width, deflection at midspan, stress and strain in prestressing steel, reinforcing steel, and concrete. Observations and experimental results were discussed.

5.2 Conclusions

Based on the results of the experimental program, the following conclusions can be drawn:

1. The tendon profile and loading type of hybrid beams greatly affect the beams overall deflection and the flexural reinforcement strain.

2. The tendon profile affects the overall capacity of the beam. One-point tendon profiles tend to have higher capacity than two-point tendon profiles.

3. The loading type affects the deflection. Two-point loading tends to have higher deflection.

4. ACI 318-14 (2014) does not provide an equation that can address the presence and a combination of unbonded and bonded tendons for hybrid beams. While AASHTO (2017) addresses the situation when bonded and unbonded tendons are present in hybrid beams, there is a need to verify the accuracy of such approach using additional experimental results from tests on continuous beams.

5. It is recommended that further studies be carried out to verify the experimental results and further investigate other parameters of hybrid continuous beams.

6 REFERENCES

1. *AASHTO LRFD Bridge Design Specifications*. American Association of State Highway and Transportation Officials, 2017.
2. Abu-Obeidah, A. "Flexural Behavior of Concrete Beams Prestressed with Bonded and Unbonded Tendons." *Rutgers University*, 2017.
3. ACI Committee 318, "Building Code Requirements for Reinforced Concrete (ACI 318-08)," American Concrete Institute, Detroit, Michigan, 2008.
4. ACI Committee 440, "Prestressing Concrete Structures with FRP Tendons (ACI 440.4R-04)," American Concrete Institute, Farmington Hills, MI, 2004.
5. Au, F. T. K., and J. S. Du. "Prediction of Ultimate Stress in Unbonded Prestressed Tendons." *Magazine of Concrete Research*, vol. 56, no. 1, 2004, pp. 1–11., doi:10.1680/macr.56.1.1.36288.
6. Beitelman, T. (2000). Tensile test results of post tensioning cables from the midbay bridge. Niceville: Structures Research Center, Florida Department of Transportation .
7. Bondy, K. (2006). Evaluation and repair of existing post-tensioned buildings with paper wrapped tendons experiencing corrosion damage. PTI Journal, 4(2), 24-29.
8. Brenkus, N. R. "Ultimate Strength of Post-Tensioned Girders with Mixed Bonded and Unbonded Prestressing." *University of Florida*, 2016.
9. British Standards Institution, "Structural Use of Concrete," BS 8110, BSI, London, 2001
10. Burningham, C. A., et al. "Repair of Prestressed Concrete Beams with Damaged Steel Tendons Using Post-Tensioned Carbon Fiber- Reinforced Polymer Rods." *ACI Structural Journal*, vol. 111, no. 2, 2014, doi:10.14359/51686529.
11. *Design of Concrete Structures*. CSA Group, 2015.
12. El Meski, F., and M. Harajli. "Flexural Capacity of Fiber-Reinforced Polymer Strengthened Unbonded Post-Tensioned Members." *ACI STRUCTURAL JOURNAL* , vol. 111, 2014.
13. Gerges, N, and Gergess, A. N. "Implication of Increased Live Loads on the Design of Precast Concrete Bridge Girders." *PCI Journal*, vol. 57, no. 4, 2012, pp. 78–95., doi:10.15554/pcij.09012012.78.95.
14. Ghallab, A., and Beeby, A. W. "Deflection of Prestressed Concrete Beams Externally Strengthened Using Parafil Ropes." *Magazine of Concrete Research*, vol. 55, no. 1, 2003, pp. 1–17., doi:10.1680/macr.2003.55.1.1.
15. Ghallab, A. and Hassan A. "Strengthening Prestressed Beams Using Parafil Ropes as External Tendons." *The University of Leeds, Woodhouse Lane Leeds, UK*, 2001.
16. Ghallab, A., and Beeby, A.W. "Factors Affecting the External Prestressing Stress in Externally Strengthened Prestressed Concrete Beams." *Cement and Concrete Composites*, vol. 27, no. 9-10, 2005, pp. 945–957., doi:10.1016/j.cemconcomp.2005.05.003.
17. Han, M. Y., et al. "Prestressed Concrete Girder with Multistage Prestressing Concept." *ACI Structural Journal*, vol. 100, no. 6, 2003, doi:10.14359/12838.

18. Harajli, M H. “Effect of Span-Depth Ratio on the Ultimate Steel Stress in Unbonded Prestressed Concrete Members.” *ACI Structural Journal*, vol. 87, no. 3, 1990, pp. 305–312., doi:10.14359/2631.
19. He, Z., and Zhao Liu. “Stresses in External and Internal Unbonded Tendons: Unified Methodology and Design Equations.” *Journal of Structural Engineering*, vol. 136, no. 9, 2010, pp. 1055–1065., doi:10.1061/(asce)st.1943-541x.0000202.
20. Hussien, O.f., et al. “Behavior of Bonded and Unbonded Prestressed Normal and High Strength Concrete Beams.” *HBRC Journal*, vol. 8, no. 3, 2012, pp. 239–251., doi:10.1016/j.hbrcj.2012.10.008.
21. Li, D., and Kaewunruen, S. “Effect of Extreme Climate on Long-Term Performance of Railway Prestressed Concrete Sleepers.” *Proceedings*, vol. 2, no. 16, 2018, p. 1146., doi:10.3390/proceedings2161146.
22. Lou, T, et al. “Response of Continuous Concrete Beams Internally Prestressed with Unbonded FRP and Steel Tendons.” *Composite Structures*, vol. 154, 2016, pp. 92–105., doi:10.1016/j.compstruct.2016.07.028.
23. Mattock, A.H., et al. “Comparative Study of Prestressed Concrete Beams, With and Without Bond.” *ACI Journal Proceedings*, vol. 68, no. 2, 1971, doi:10.14359/11298.
24. Naaman, A. E, and Alkhairi, F.M. “Stress at Ultimate in Unbonded Post-Tensioning Tendons: Part 2--Proposed Methodology.” *ACI Structural Journal*, vol. 88, no. 6, 1992, doi:10.14359/1288.
25. Namman, A E, and Alkhairi F.M. “Stress at Ultimate in Unbonded Post-Tensioning Tendons: Part 1--Evaluation of the State of the Art.” *ACI Structural Journal*, vol. 88, no. 5, 1991, pp. 641–651., doi:10.14359/2763.
26. Namman, A. E, et al. “Stresses in Unbonded Prestressing Tendons at Ultimate: Recommendation.” *ACI Structural Journal*, vol. 99, no. 4, 2002, pp. 518–529., doi:10.14359/12121.
27. Osimani , F. “The Use of Unbonded Tendons for Prestressed Concrete Bridges .” *Royal Institute of Technology* , 2004.
28. Ozkul, O, Nassif, H., Tanchan, P. , and Harajli, M. “Rational Approach for Predicting Stress in Beams with Unbonded Tendons.” *ACI Structural Journal*, vol. 105, no. 3, May 2008, pp. 338–347., doi:10.14359/19793.
29. Ozkul, O. “A New Methodology for the Analysis of Concrete Beams Prestressed with Unbonded Tendons.” *Rutgers, The State University of NJ, New Brunswick, NJ*, 2007.
30. Pannell, F. N. “The Ultimate Moment of Resistance of Unbonded Prestressed Concrete Beams.” *Magazine of Concrete Research*, vol. 21, no. 66, Mar. 1969, pp. 43–54., doi:10.1680/macr.1969.21.66.43.
31. Seguirant, S. J., et al. “Flexural Strength of Reinforced and Prestressed Concrete T-Beams.” *PCI Journal*, vol. 50, no. 1, 2005, pp. 44–73., doi:10.15554/pcij.01012005.44.73.
32. Shahawy, M. A., and Barrington D. B. “Shear Behavior of Full-Scale Prestressed Concrete Girders: Comparison Between AASHTO Specifications and LRFD Code.” *PCI Journal*, vol. 41, no. 3, 1996, pp. 48–62., doi:10.15554/pcij.05011996.48.62.

33. Six, P. D. “Continuous Unbonded Post-Tensioned Members: Quantifying Strand Stress Increase.” *Utah State University*, 2015.
34. Tanchan, P. “Flexural Behavior of High Strength Concrete Beams Prestressed with Unbonded Tendons.” *Rutgers, The State University of NJ, New Brunswick, NJ*, 2001.
35. Unal, G. “Simplified Prediction Equation for Ultimate Stress in Beams Prestressed with Hybrid Tendons.” *Rutgers University*, 2011.
36. United States, Congress, “AASHTO LRFD Bridge Design Specifications.” *AASHTO LRFD Bridge Design Specifications*, American Association of State Highway and Transportation Officials, 2010.
37. United States, Congress, “Design of Concrete Structures.” *Design of Concrete Structures*, CSA Group, 2015.
38. Zheng, W., and Wang, X-D. “Ultimate Stress Increase in Unbonded Tendons in Prestressed Concrete Beams.” *Journal of Zhejiang University-SCIENCE A*, vol. 11, no. 12, 2010, pp. 998–1014., doi:10.1631/jzus.a0900618.
39. Zhou, W., and Zheng, W. “Unbonded Tendon Stresses in Continuous Post-Tensioned Beams.” *ACI Structural Journal*, vol. 111, no. 3, 2014, doi:10.14359/51686569.
40. Zhou, W., and Xie, X. “Flexural Response of Continuous Unbonded Post-Tensioned Beams Strengthened with CFRP Laminates.” *Composite Structures*, vol. 211, 2019, pp. 455–468., doi:10.1016/j.compstruct.2019.01.003.